Original Article

Trends in Hearing
Volume 22: 1–11

DOI: 10.1177/2331216518774450
journals.sagepub.com/home/tia
SAGE

PVDF-Based Piezoelectric Microphone for Sound Detection Inside the Cochlea: Toward Totally Implantable Cochlear Implants

Steve Park[1], Xiying Guan[2], Youngwan Kim[3], Francis (Pete) X. Creighton[2], Eric Wei[4], Ioannis (John) Kymissis[3], Hideko Heidi Nakajima[2], and Elizabeth S. Olson[4,5]

Abstract

We report the fabrication and characterization of a prototype polyvinylidene fluoride polymer-based implantable microphone for detecting sound inside gerbil and human cochleae. With the current configuration and amplification, the signal-to-noise ratios were sufficiently high for normally occurring sound pressures and frequencies (ear canal pressures >50–60 dB SPL and 0.1–10 kHz), though 10 to 20 dB poorer than for some hearing aid microphones. These results demonstrate the feasibility of the prototype devices as implantable microphones for the development of totally implantable cochlear implants. For patients, this will improve sound reception by utilizing the outer ear and will improve the use of cochlear implants.

Keywords

cochlear implant, microphone, piezoelectric, PVDF

Date received: 13 November 2017; revised: 7 April 2018; accepted: 9 April 2018

Introduction

According to the Global Hearing Implants Market Outlook 2020 report, the hearing implants market will reach $2.9 billion by 2020, with cochlear implants (CIs) projected to occupy the largest share. CIs are neural prosthetic devices that restore a sense of hearing to severe to profoundly deaf individuals. According to the National Institute on Deafness and Other Communications Disorders, as of 2012 an estimated 324,000 people received CIs worldwide, with about 96,000 CI users in the United States alone, making CIs the most implanted neural prosthetic devices.

Individuals requiring CIs typically suffer from damaged or missing cochlear hair cells. The primary role of hair cells is to convert sound-driven intracochlear vibration into electrical signals, which subsequently stimulate the auditory neurons. CIs work by picking up sound using a microphone located externally above the pinna, and with an external processor, convert the microphone output into electrical pulses that are transmitted internally using a transmitter or receiver to finally stimulate the auditory neurons using an array of electrodes implanted in the cochlea. Despite the improvements in CIs in recent years (Crathorne et al., 2012; Wilson & Dorman, 2008a, 2008b; Zeng, Rebscher, Harrison, Sun, & Feng, 2008), CIs still have a number of limitations. One of the main limitations is CI users' difficulty hearing in the midst of multiple sound sources. This is in part due to the lack of sound localization

[1]Department of Materials Science and Engineering, Korea Advanced Institute of Science and Technology, Daejeon, Republic of Korea
[2]Department of Otolaryngology, Harvard Medical School, Massachusetts Eye and Ear, Boston, MA, USA
[3]Department of Electrical Engineering, Columbia University, New York City, NY, USA
[4]Department of Otolaryngology Head and Neck Surgery, Columbia University Medical Center, New York City, NY, USA
[5]Department of Biomedical Engineering, Columbia University, New York City, NY, USA

Corresponding author:
Steve Park, Korea Advanced Institute of Science and Technology, 291 Daehak-ro, Yuseong-gu, Daejeon, 34141, Republic of Korea.
Email: stevepark@kaist.ac.kr

capability of CIs because of the location of the external microphone (without the advantage of the outer ear for directionality). Another limitation of CIs is the presence of external components that render the use of CIs difficult under various situations such as sporting activities. Users typically cannot wear CIs during sleep, preventing hearing at all times, which impacts children's brain development. The external component of the CI can be a cosmetic issue and a discomfort for patients, and the daily maintenance and positioning required of the external component can be inconvenient and difficult for the very young and elderly. A totally implantable CI device would address these issues, but requires overcoming several technical hurdles including miniaturized and low-power electronics (Yip, Jin, Nakajima, Stankovic, & Chandrakasan, 2015) and implantable microphones. Implantable microphones in particular would improve current CI systems by making use of the acoustic cues produced by the outer ear and ear canal. An implanted microphone will result in improved binaural cues and generate a signal that better represents normal hearing to CI users. In addition to its primary signal transduction role, the implanted microphone can also serve as a monitoring device useful for implant placement and maintenance. An implantable device could, for example, provide information about postimplantation scarring by measuring the intracochlear sound pressure. As another example, the intracochlear pressure might undergo an abrupt change upon stimulation of the stapedius muscle reflex, and using the implanted microphone to detect the stapedius muscle contraction could be used for setting the correct stimulus range in young children.

In this article, we report on an intracochlear microphone based on the piezoelectric polymer PVDF (polyvinylidene fluoride) that detects the sound pressure inside the fluid-filled cochlea. PVDF has high elastic compliance, high resistance to radiation and chemicals that allow sterilization before implantation, and a broadband frequency sensitivity that covers the human speech range. Because PVDF can be shaped into various shapes and dimensions, the desired devices can be readily fabricated. PVDF has previously been used in a variety of applications such as cardiorespiratory monitoring (Choi & Jiang, 2006), energy harvesting devices (Cha et al., 2011; Mao et al., 2014; Pi, Zhang, Wen, Zhang, & Wu, 2014; Yu et al., 2016; Zabek, Taylor, Boulbar, & Bowen, 2015), tactile sensing (Khan, Tinku, Lorenzelli, & Dahiya, 2015; J. S. Lee, Shin, Cheong, Kim, & Jang, 2015; Persano et al., 2013), acoustic sensing (Chocat et al., 2012; Lang, Fang, Shao, Ding, & Lin, 2016; Xu, Dapino, Gallego-Perez, & Hansford, 2009), and textile sensing (Åkerfeldt, Lund, & Walkenström, 2015; Krajewski, Magniez, Helmer, & Schrank, 2013; Nilsson, Lund, Jonasson, Johansson, & Hagström, 2013). PVDF and other piezoelectric materials have been used to make biomimetic artificial hair cells; however, these devices generally are not configured as practical medical devices (Inaoka et al., 2011; H. S. Lee et al., 2014). Other groups have built piezoelectric sensors from ceramic piezoelectrics for cochlear sensing and actuation (Luo et al., 2015; Zhao, Knisely, & Grosh, 2017) and an implantable microphone based on a microelectromechanical systems (MEMS) condenser microphone is under development (Pfiffner et al., 2017). In this article, we describe the development and multifaceted testing of a simple, robust PVDF sensor for measuring intracochlear pressure, which could be a component of a totally implantable CI.

Results

β-phase PVDF thin-films, 50 μm in thickness, were provided by Measurement Specialties, Norristown PA. The β-phase crystalline structure can be obtained by mechanical stretching along the one-direction and poling along the three-direction by applying a strong electric field at high temperatures, then lowering the temperature to lock the domains in their poled state (Figure 1(a); Dickens, Balizer, Dereggi, & Roth, 1992; Li, Kagami, & Ohigashi, 1992). Sixty to hundred nanometers thick patterned Au or Ag contacts were deposited on the top and bottom surface of the PVDF film using shadow masking (Figure 1(b)). The area where the two electrodes overlap is the capacitor that generates the surface charges used for voltage measurement, which we hereon refer to as the active area. Due to the roughness of the PVDF surface, an electrode width greater than 100 μm was needed to prevent the electrodes from breaking and generating an open circuit. In another set of devices, Au or Ag contacts were deposited without shadow masking, in which case the entire area of the device was the active area.

Figure 1(c) is a plot of the capacitance of a patterned PVDF device with an active area of 33 mm^2, as a function of frequency from 100 to 50,000 Hz. Supplementary Figure S1 shows the dielectric permittivity and dissipation factor versus frequency plot (source: Measurement Specialties). Since the relative dielectric constant of PVDF is 12 to 13, the predicted capacitance of this PVDF device was ~70 pF, and we confirmed this value experimentally. The capacitance decreased slightly above 15 kHz. However, at 50 kHz, the drop was only 14%, and reduced sensitivity was not apparent in our calibrations to at least 40 kHz (Figure 3). The full frequency range for human hearing is 20 to 20,000 Hz.

The general equation of electric displacement D (coulomb/m^2) along the three-direction for a PVDF film that is unidirectionally poled along the

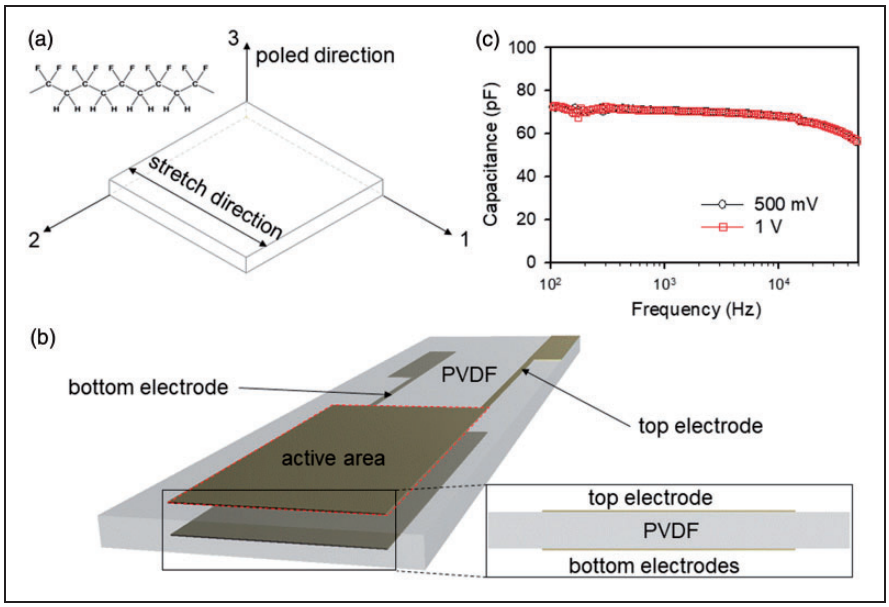

Figure 1. (a) Molecular structure of β-phase PVDF and a schematic depiction of PVDF film with labeled axes. (b) Schematic of PVDF device with electrodes patterned on top and bottom surface of PVDF film. The overlapping area is the active area where surface charge or voltage is measured. (c) Capacitance as a function of frequency of a PVDF device measured with applied voltages of 0.5 V and 1 V.

three-direction (in the absence of externally applied electric field) is,

$$D_3 = \sum_{j=1}^{3} d_{3j}\sigma_j \tag{1}$$

where d_{3j} is the piezoelectric strain constant with the left subscript indicating internal electric field direction and the right subscript indicating stress direction, and σ_j is the applied pressure with the subscript indicating stress direction. For a purely compressive mode along the three-direction, Equation (1) reduces to $D_3 = d_{33}\sigma_3$, whereas for a purely stretch mode along the one-direction, Equation (1) reduces to $D_3 = d_{31}\sigma_1$. The specified values of d_{33} and d_{31} of PVDF are -33×10^{-12} and 23×10^{-12} C/N, respectively. Normally, to generate σ_1 under bending, the PVDF film needs to be attached on a thicker material so that the neutral axis is outside of the PVDF film. The total voltage generated across the PVDF film (V_{PVDF}) is given by,

$$V_{PVDF} = \frac{D_3}{c_{PVDF}} = \frac{D_3}{\epsilon_o \epsilon_{PVDF}/t_{PVDF}} \tag{2}$$

where c_{PVDF} is the capacitance per unit area, ϵ_0 is the permittivity of free space, ϵ_{PVDF} is the relative dielectric constant of PVDF, and t_{PVDF} is the thickness of the PVDF sheet. Assuming pure compression (i.e., $D_3 = d_{33}\sigma_3$), the intrinsic pressure sensitivity (V/Pa) of the PVDF film is predicted to be 15.5 μV/Pa. This value, according to Equation (2), is independent of the size of the active area; however, the measured output voltage will only attain this value if the sensor is not loaded electrically (e.g., it connects to a very high impedance amplifier or buffer, as we discuss quantitatively below).

Figure 2(a) is a circuit diagram of the PVDF device connected to an amplifier. Equation (3) expresses the voltage going into an amplifier (V_{IN}), which depends not only on the voltage generated by the PVDF (V_{PVDF}) but also on the relative values of the output impedance of the PVDF device ($Z_{O.PVDF}$) and the input impedance of the amplifier ($Z_{I.AMP}$).

$$\begin{aligned} V_{IN} &= V_{PVDF}\frac{Z_{I.AMP}}{Z_{I.AMP} + Z_{O.PVDF}} \\ &= V_{PVDF}\frac{(j\omega C_I + 1/R_I)^{-1}}{(j\omega C_I + 1/R_I)^{-1} + (j\omega C_{PVDF})^{-1}} \end{aligned} \tag{3}$$

The output impedance of the PVDF sensor ($Z_{O.PVDF}$) is primarily capacitive, equal to $1/(j\omega C_{PVDF})$, where ω is the angular frequency in radians. The input impedance of our amplifier, based on the specifications (PARC EG&G) is modeled as a 100 MΩ resistor (R_I) and a 15 pF capacitor (C_I) in parallel; therefore, $Z_{I,AMP} = (j\omega C_I + 1/R_I)^{-1}$. The voltage amplifier that we have used was reasonable for initial bench testing due to its low noise and high input impedance; however, we note that another amplifier (e.g., a charge amplifier)

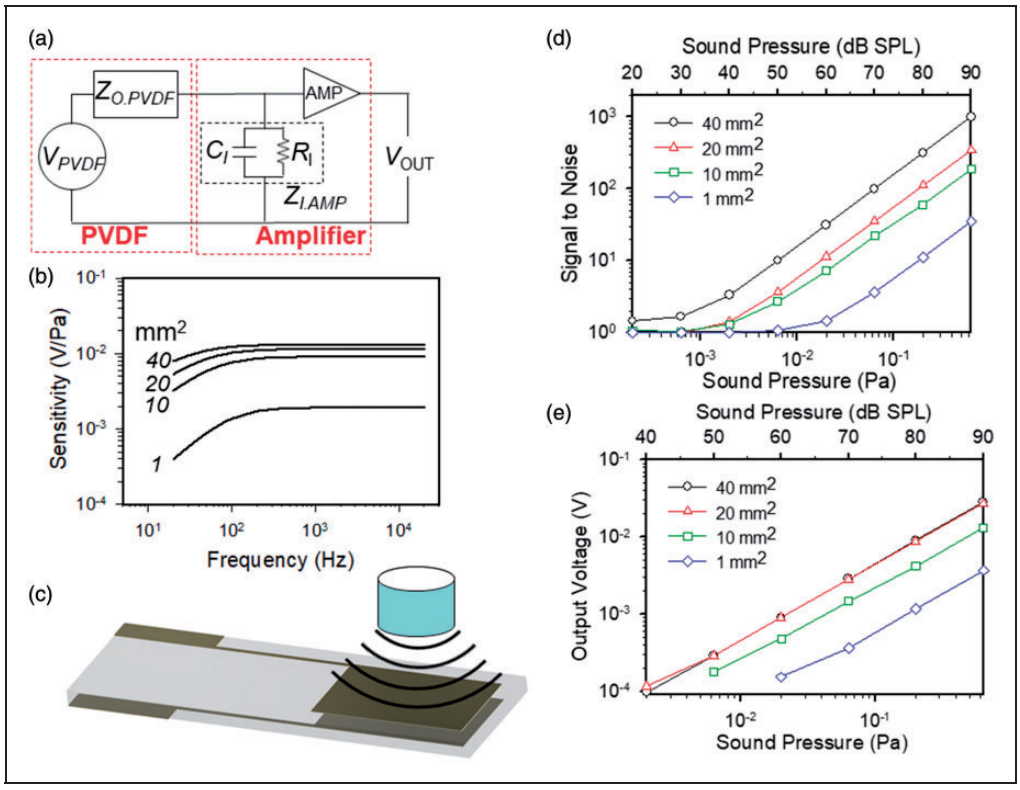

Figure 2. (a) Circuit diagram of PVDF device connected to an amplifier. (b) Expected sensitivity (V/Pa) as a function of frequency of PVDF devices with different active areas (40, 20, 10, and 1 mm^2), when amplified with a PARC amplifier with a gain of 1,000. Pure compression mode (d_{33}) is assumed. (c) Schematic depiction of PVDF device being stimulated with sound pressure. (d) Plot of signal-to-noise ratio as a function of sound pressure for devices with different active areas. (e) Plot of output voltage (with amplifier gain of 1,000) as a function of sound pressure for devices with different active areas. Data points close to the noise level were omitted. For (d) and (e), output voltage from 10 to 20 kHz were averaged, and the noise and pickup level were measured with the sound source removed. The *x*-axes in (d) and (e) are labeled in both dB SPL and Pa. The conversion is dB SPL = 20log(P/20 μPa).
PVDF = polyvinylidene fluoride.

should likely be used for implementation in CIs. Figure 2(b) is the expected sensitivity versus frequency plot, assuming pure compression and with PARC gain of 1,000, for PVDF devices with different active areas: 40, 20, 10, and 1 mm^2. As the size of the active area gets smaller, the predicted output voltage decreases. This is due to decreasing C_{PVDF} with decreasing active area, which in turn will increase the output impedance of the PVDF device. Also, for all of the devices, the output voltage decreases as frequency decreases due to the increase in output impedance of the PVDF device as frequency decreases in comparison to the input impedance of the amplifier, which saturates at R_I. The half power points (frequency at which output voltage drops by $1/\sqrt{2}$) for PVDF devices with active areas equal to 40, 20, 10, and 1 mm^2 are 29.3, 44.4, 61.2, and 98.1 Hz, respectively.

Since our devices need to be inserted into the cochlea, the width of our device is limited by the diameter of the round window and scala tympani (ST), which is ~0.5 mm for gerbil and ~2 mm for human cochleae. Such a limitation in width sets a limit on the size of our active area, which, as described above, can compromise the output voltage signal. Hence, we conducted preliminary testing on the dependence of output voltage and signal-to-noise ratio (SNR) on the active area. Sound of varying pressure was applied to each PVDF device by connecting one end of a rubber tube to a speaker and suspending the other end of the tube at a fixed height above the PVDF devices (Figure 2(c)). The devices were firmly taped to glass slides to predominantly restrict them to strain along the three-direction (compression). The induced sound was calibrated using a commercially available microphone (Sokolich ultrasonic microphone). For each sound pressure, tones of frequency ranging from 10 to 20 kHz were applied in steps of 100 Hz (Supplementary Figure S2). The tones were 1 s in duration and the amplitudes of the responses were found after conducting a fast Fourier transform of the measured responses. To minimize electromagnetic pickup, we placed the PVDF device in a grounded aluminum box. The speaker was outside of the box and its acoustic output was delivered via a rubber tube. The noise and pickup level was found by

measuring the output voltage with the tube removed. Supplementary Figure S3 shows the reduction in pickup level with the PVDF device in a grounded aluminum box. Figure 2(d) and (e) shows the plots of SNR and output voltage (with gain of 1,000) found by taking the average response over the 10 to 20 kHz range at each sound pressure level. The sensitivity of the devices can be calculated from the slope of the plot in Figure 2(e), which is 45, 43, 21, and 6 mV/Pa for devices with active area equal to 40, 20, 10, and 1 mm^2, respectively. These values are within about a factor of 3 of the expected sensitivity values from Equation (3) (13.5, 11.5, 9.08, and 1.98 mV/Pa for devices with active area equal to 40, 20, 10, and 1 mm^2, respectively). The experimental values are slightly larger than the expected, which may have resulted from imprecision in sound calibration. The agreement between measurement and prediction is reasonable. As predicted by Equation (3), with decreasing active area, both the sensitivity and SNR decreases. This effect sets a limit on the minimum sound pressure that can be detected. For the device with 1 mm^2 active area, the sound pressure detection limit was 60 dB SPL, whereas for devices with larger active area, sound pressures down to 40 dB SPL were detected. These results confirm the importance of device size for attaining reasonably high output voltage signal and SNR at normally occurring sound frequencies and pressures. The results also highlight the desire for a high-input impedance amplifier or a charge amplifier for the first stage of signal amplification, and the benefit of the development of lower output impedance PVDF devices. These topics are subjects of our future work.

Because the cochlea is fluid-filled, the PVDF device needs to be encapsulated with an insulator to prevent the shorting of the electrodes. Therefore, we fabricated the device as seen in Figure 3(a) and (b). A PVDF device of 0.5 mm and 15 mm in width and length (area ~7.5 mm^2) was fabricated with the top and bottom electrodes covering the entire area of the device to maximize the active area, thereby maximizing output voltage. The dimensions were chosen so that the device can fit along the length of human cochleae. This PVDF device was then injection molded into a 0.6 mm diameter PDMS (polydimethylsiloxane) cylinder (Platsil 71-11 RTV silicon rubber, Polytek, Easton PA). Silicone rubber is used to encapsulate conventional CIs, which are meant to last a lifetime. The properties and longevity of the materials used in CIs have been previously

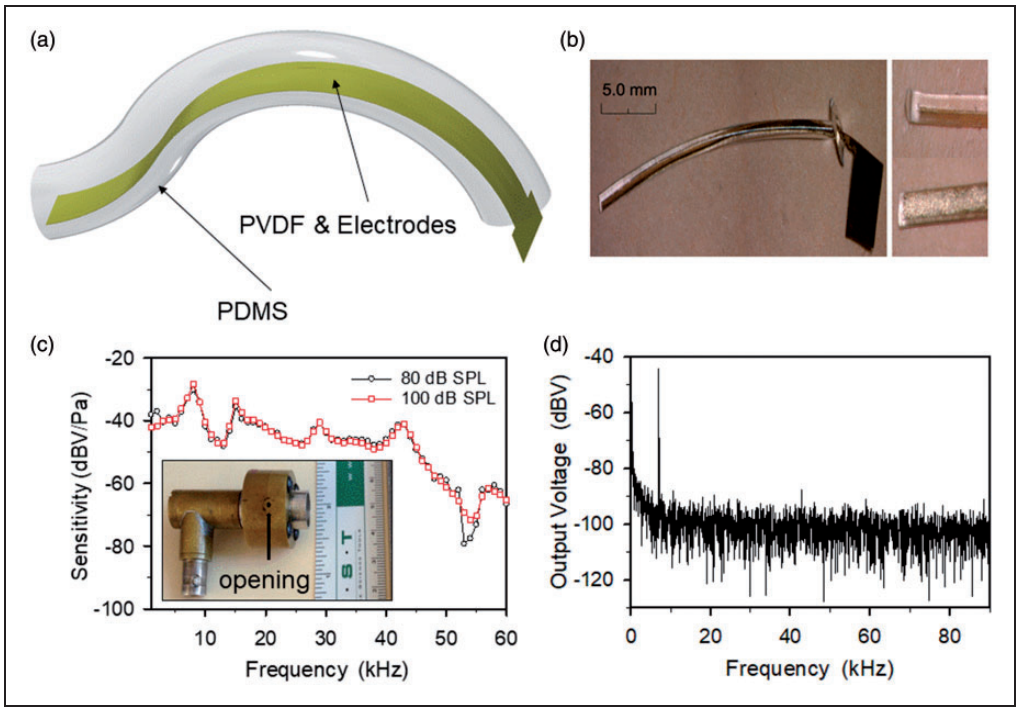

Figure 3. (a) Schematic of a PVDF device encapsulated in PDMS cylinder. The length and width of the PVDF film were 15 mm and 0.5 mm, respectively. The diameter of the PDMS cylinder was 0.6 mm. (b) Optical image of the PVDF device encapsulated in PDMS cylinder. (c) Plot of sensitivity as a function of sound frequency for a PVDF device inside an air pressure chamber. Sound pressure was delivered at two levels, 80 and 100 dB SPL. Inset is an image of the air pressure chamber. The PVDF device was inserted into the small opening indicated by the black arrow. (d) Spectral plot (after a gain of 1,000 using the voltage amplifier described in Figure 2) of the response to a sound delivered at 80 dB SPL and 7 kHz.
PDMS = polydimethylsiloxane; PVDF = polyvinylidene fluoride.

reviewed (Stöver & Lenarz, 2009). The injection molding procedure was as follows: After mixing the PDMS two-part formulation, it was degassed with a vacuum pump and then pulled (using pump-generated suction) into rubber tubes of inner diameter 0.6 mm that held the metal-deposited PVDF strips. After curing (typically overnight at room temperature), the outer rubber tube was sliced open with a blade to release the encapsulated PVDF device. We firstly tested the devices in an air pressure chamber, as seen in the inset of Figure 3(c). The encapsulated PVDF device was inserted into the small opening indicated by the arrow. The chamber was connected to both a speaker (BNC connection on bottom) and a Bruel and Kjaer ¼″ microphone (would be connected on the right). Figure 3(c) is a plot of sensitivity (dBV/Pa) versus sound frequency with a gain of 1,000. The stimulus frequency varied from 1 to 60 kHz and the pressure level was 80 and 100 dB SPL. The PDMS-embedded sensor is expected to experience a complex and frequency-dependent strain field. The response in Figure 3(c) shows peaks and valleys, with the first resonance at ~8 kHz, that are likely due to mechanical resonances in the PDMS cylinder. Therefore, there is not a simple prediction for the voltage output, as we have done for Figure 2(d) and (e) (i.e., a single sensitivity value cannot be defined over a broad range of frequencies). Figure 3(d) is a spectral plot of the response to a pressure of 80 dB SPL at 7 kHz (the most sensitive frequency), showing SNR of ~45 dB, measured with a 1 Hz bandwidth. The SNR value will differ at different frequencies due to the peaks and valleys in the signal, as seen in Figure 3(c). From 1 to 40 kHz, at 80 dB SPL, the average SNR was ~30 dB. Hence, sound pressure needs to be above ~50 dB SPL for SNR > 1.

We conducted further testing of the device in vivo in the cochlea of a gerbil, as seen in Figure 4. The gerbil is a rodent often used in auditory research. The animal was anesthetized and surgery was performed to expose the cochlea. At the end of the experiment, the gerbil was euthanized with an overdose of anesthetic. The procedures were approved by Columbia University's Institutional Animal Care and Use Committee. Once anesthetized, sound was delivered to the ear canal with a closed sound system that also contained a microphone for monitoring the sound level. Intracochlear pressure was measured with a fiber optic pressure sensor devised for such measurements and details on that pressure sensor and the animal preparation can be found in Olson (1998). Because the PVDF sensor was too large

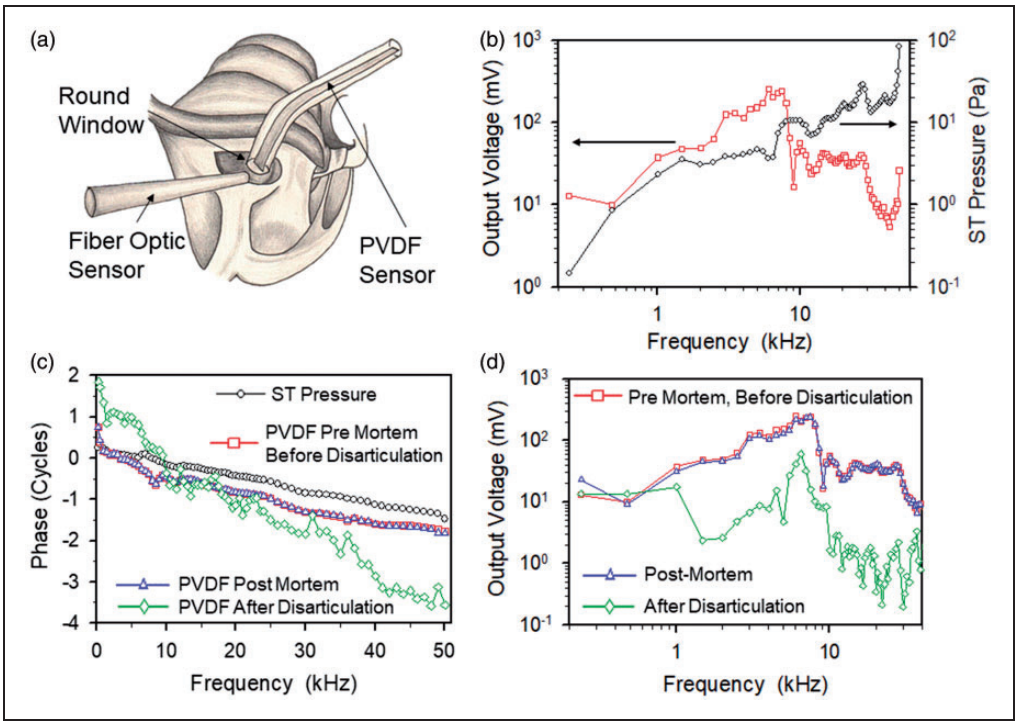

Figure 4. (a) Schematic of fiber optic and PVDF pressure sensor inserted into the round window of a gerbil cochlea. (b) Plot of output voltage (after a gain of 1,000) measured with PVDF sensor (red square) and pressure in the scala tympani measured with fiber optic pressure sensor (black circle). (c) Plot of phase measured with fiber optic pressure sensor (black circle), PVDF sensor premortem and before disarticulation (red squares), postmortem (blue triangles), and after disarticulation (greed diamonds). (d) Plot of output voltage (after a gain of 1,000) measured with PVDF sensor premortem or before disarticulation (red squares), postmortem (blue triangles), and after disarticulation (green diamonds).
PVDF = polyvinylidene fluoride.

to be inserted deeply into the gerbil cochlea, this was simply a test that pressures within the cochlear fluids could be monitored with the PVDF sensor and that the device did not problematically pickup the cochlea's hair cell-based responses to sound, or the electrical signals driving the speaker. Figure 4(a) shows a schematic of the PVDF device placed just within the cochlea's round window opening after removing the round window membrane. The sound pressure delivered to the ear canal was 100 dB SPL, over a range of frequency from 0.2 to 50 kHz. The fiber optic pressure sensor was used first and was inserted approximately 0.5 mm down the cochlear spiral in the ST, which is a location fairly close to the round window opening. It measured the intracochlear sound pressure shown as black circles in Figure 4(b). The intracochlear pressure at this location is relatively small at the lower frequencies due to the mass-dominated mechanical impedance to *pressure ground* at the round window. The linearly decreasing phase versus frequency in Figure 4(c) (black circle) is the familiar middle ear delay, with a value of ~25 to 30 μs in gerbil. The red squares in Figure 4(b) show the output voltage measured with the PVDF device. Ideally, the frequency response measured with the PVDF sensor would align with the pressure frequency response measured with the fiber optic sensor. The phase versus frequency response measured with the PVDF sensor (red square) in Figure 4(c) shows the familiar linearly decreasing phase due to the middle ear delay. This provides compelling evidence that the PVDF sensor was primarily measuring intracochlear responses (as opposed to the sound signal in the air or electromagnetic pickup from speaker). The PVDF sensor amplitude in Figure 4(b) tracks the pressure as measured with the fiber optic sensor well until ~9 kHz, where there is a notch and drop-off of more than 10 dB. This additional frequency structure in the PVDF sensor response could be due to the fact that the PVDF was not inserted as deeply into the cochlea as the fiber optic sensor, or might be due to a resonance in the PDMS-embedded device, since such resonant behavior was apparent in Figure 3. The average sensitivity of the PVDF sensor below 9 kHz was 20 mV/Pa. This value was twice as large as the predicted value from Equation (3), 9 mV/Pa. The difference in these values is again likely due to the complex and frequency-dependent strain field of a PDMS-embedded sensor. Furthermore, the pressure gradients close to the round window opening might have caused additional complex behavior. Further study is required to understand these complex vibration modes and is a subject of future work.

As seen in Figure 4(c) and (d), the phase and output voltage of the PVDF sensor output did not change postmortem (blue triangles), and this is as expected since the sensor was distant from the sensory tissue. Also, this indicated that the sensor was not picking up the cochlea's hair-cell-based electrical activity, since this disappears rapidly postmortem. Upon disarticulating the ossicular chain (e.g., middle ear), the sensor response fell by ~20 dB over most frequencies, while the phase was no longer aligned with previous measurements (green diamonds). This is as expected since the middle ear drives the cochlea and generates most of the intracochlear pressure. It also demonstrates that the original measurements with articulated middle ear were not artifact (e.g., not electromagnetic pickup from the speaker). Overall, this in vivo test showed that there were no unanticipated problems with an intracochlear measurement and encouraged the next set of tests in fresh human cadaveric temporal bones.

Figure 5(a) is a schematic of the experimental setup of the sound pressure measurement inside the human cochlea. A charge amplifier was used in these experiments, with sensitivity of 0.2 V/pC (C = coulomb). (Note: The input impedance of a charge amplifier does not need to be taken into consideration, since the input is a virtual ground, with output voltage proportional to charge delivered to the virtual ground.) Sound was delivered to the ear canal, and a hearing aid microphone (Etymotic) was used to measure the sound in the ear canal. The PVDF device was inserted into the ST through the round window as shown in Figure 5(b). The PVDF microphone was nearly fully inserted into the cochlea, similar to the surgical insertion of a CI. We published a related set of temporal bone results recently in a clinical journal to show proof of concept without technical details (Creighton et al., 2016) and the results here are from a similar device on a different experimental day and different temporal bone. Figure 5(c) is a plot of output voltage as a function of frequency, with the speaker driven at a frequency-independent voltage level at seven different attenuations, separated by 5 dB. Note that in Figure 5(c), voltage drive, not sound level was fixed in frequency. Linearity of the PVDF device output was observed and is expected, since the ear is linear to very high sound levels when the cochlea is passive (as in a cadaveric specimen without the nonlinear activity from the sensory hair cells), and according to the manufacturer's technical specifications, the PVDF material is linear to extreme pressure levels >100 MPa. The peak around 180 Hz (noticeable at the lower levels) was due to the pickup of harmonics of 60 Hz noise, and improved shielding from electrical interference is a subject of our future work. Figure 5(d) is a plot of the output voltage normalized by ear canal pressure and the phase with respect to the ear canal pressure. The phase shows typical middle ear delay. Based on previous measurements of scala vestibuli and ST pressures close to the cochlear base (Nakajima et al., 2009), we can roughly estimate the ST pressure well within the cochlea (but not very close

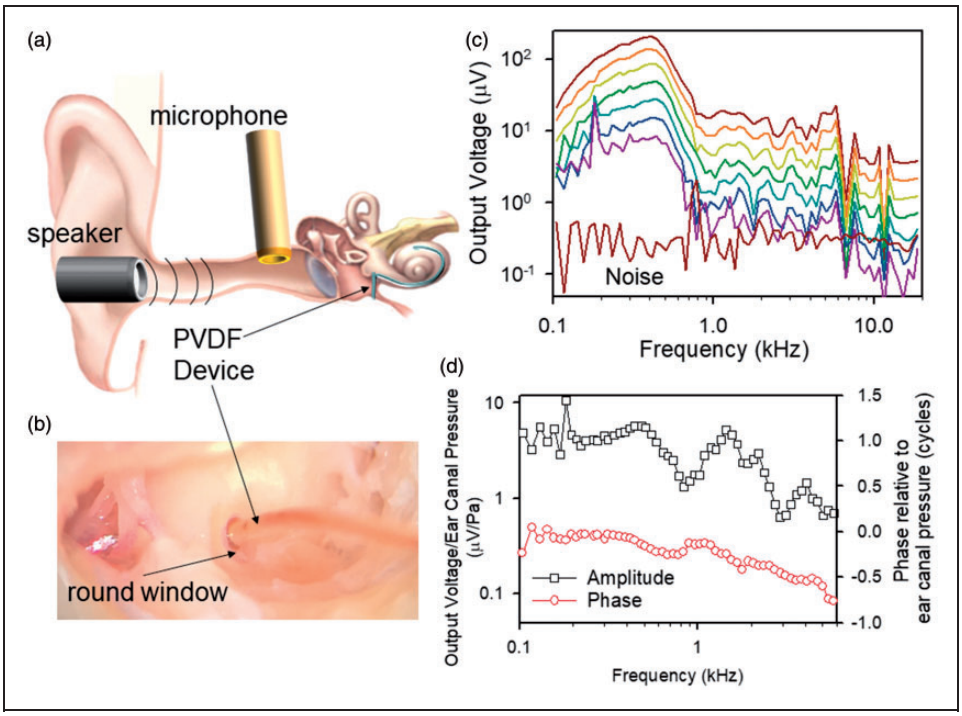

Figure 5. (a) Schematic depiction of experimental apparatus of intracochlear sound pressure measurement using PVDF device. A hearing aid microphone is used to measure ear canal pressure. (b) Image of PVDF device being inserted into the ST through the round window. (c) Plot of output voltage of PVDF versus frequency under various sound attenuations. (d) Plot of output voltage or ear canal pressure and phase relative to ear canal pressure as a function of frequency.
PVDF = polyvinylidene fluoride.

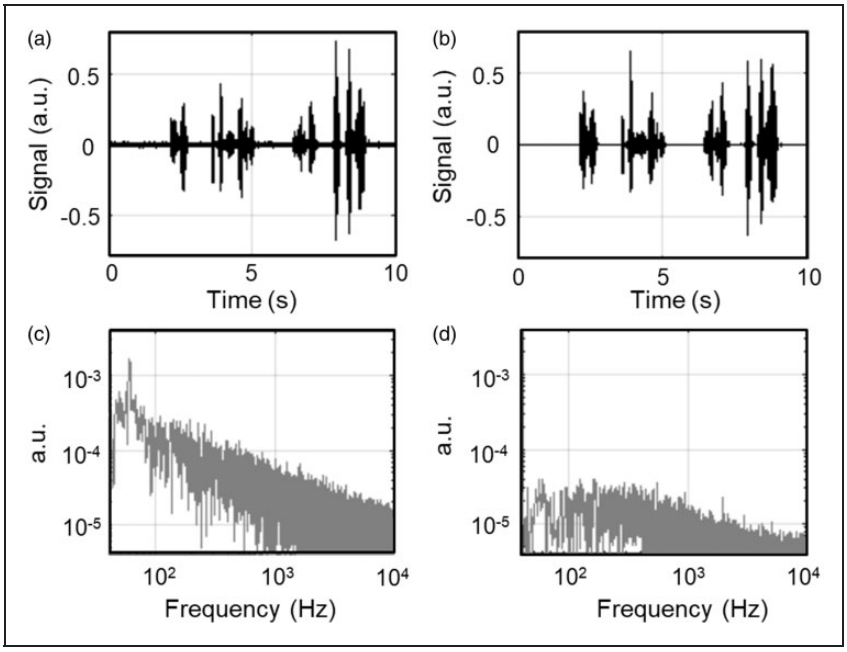

Figure 6. Time-domain responses from the (a) PVDF microphone inside cochlea and the (b) Etymotic microphone in the ear canal. Noise level for the (c) PVDF microphone and the (d) Etymotic microphone obtained by taking FFT of the first second of the time-domain response when there was no speech.
a.u. = arbitrary units.

to the sensory tissue) to be between ~0 and 10 dB greater than the pressure delivered at the ear canal. With this information and the data of Figure 5(d), in this configuration, the sensor sensitivity was ~5 μV/Pa up to a ~0.5 kHz. As a comparison, if the sensor had been operating in a pure compression mode, we would expect the following: charge amplifier factor $\times d_{33} \times$ area $= 2 \times 10^{11}$ V/C $\times 33 \times 10^{-12}$ C/N $\times 7.5 \times 10^{-6}$ m^2 $= 50$ μV/Pa. The predicted sensitivity from pure compression mode was greater than our measured sensitivity within the cochlea. Such a discrepancy is not surprising, since the stimulation, while realistic from the standpoint of how the device will be used, was not a well-controlled compressive-mode stimulation. Other factors, such as complex resonance behavior of the PDMS-embedded device and the presence of an air bubble in the cochlea cannot be ruled out.

In addition to playing tones to the ear canal, as a more illustrative check of SNR, we removed the speaker and instead spoke to the temporal bone, measuring the response with the Etymotic microphone in the ear canal and the PVDF device in the cochlea. The upper panels show the time-domain output signal to a speech signal, *I'm testing this microphone* for the PVDF device (Figure 6(a)) and the Etymotic microphone (Figure 6(b)). The two signals were scaled so that their peaks were approximately the same size. The time-domain signals were similar (they are not expected to be identical since one is measured in the ear canal and the other in the cochlea) and the speech in both audio recordings was easily discernible (Supplementary Audios). It is apparent in the audio recordings that the SNR of the PVDF microphone is lower than the SNR of the Etymotic microphone. This is quantified in Figure 6(c) and (d) by conducting fast Fourier transform of the first second of the signal (in the quiet period before speaking began) measured with the PVDF device and Etymotic microphone, respectively. Between 100 and 10,000 Hz, the SNR is ~10 to 20 dB higher for the Etymotic microphone.

Discussion and Conclusions

This study represents initial steps to develop a fully implantable CI. In a controlled setting, the PVDF-based intracochlear microphone prototype had sensitivity that was reasonably close to what was expected, based on the material's piezoelectricity and assuming compression-mode operation. To maximize the output voltage, we have maximized the device area, which inevitably eliminates the ability to make local pressure measurements. In this work, our goal was to measure the uniform compressive pressure that fills the cochlea. In fresh human cadaveric specimens, the response tended to drop at frequencies above a few kHz (Figure 5d). (The frequency response in the gerbil cochlea (Figure 4) is not worth considering in this vein, because the device was not fully inserted into the cochlea.) The reason for the high-frequency drop-off in the cadaveric experiments requires further study, including studies with independent intracochlear pressure measurements with a calibrated fiber optic sensor. Furthermore, how the signal changes with different rotations of the PVDF device should be explored. The measurements here point to an SNR in the current device that is ~10 to 20 dB too low to provide a signal as clean as that of a current high-quality hearing aid microphone. The noise in a PVDF microphone will likely be limited by the dielectric loss characteristics of the material, which is relatively high compared to piezoelectric ceramics. The loss tangent of PVDF reported by the manufacturer, Measurement Specialties, is 0.02. This is ~5 times larger than the loss tangent reported by the manufacturer APC International for a hard ceramic piezoelectric material composed of PZT (lead–zirconium–titanium). The noise level in our measurements may or may not be a PVDF-determined minimum. Optimizing the amplification was not an aim of this study, whose goal was on exploring basic feasibility. We are currently working on improving the amplification stage. We are also working on improved electrical shielding, so that the microphone can be used in conjunction with a CI. Another planned improvement is the development of piezoelectric film with higher sensitivity.

The beauty of our prototype device is its great simplicity, with CI-like size and shape. It could be incorporated into a CI with little or no change to the CI's physical properties and no change to the surgical technique. Furthermore, because our intracochlear microphone senses pressure throughout the length of the CI, it is less susceptible to limitations imposed by predictable scarring and bone growth observed especially at the base of the cochlea after CI implantation. For patients with intact middle and external ears, which is the majority of CI patients, the benefits of an intracochlear microphone are improved sound localization, ability to use their device in all activities at all times, ease of use, and cosmetic appeal. This system points the way to a bright future for fully implantable CIs.

Author Contributions

S. P., E. S. O. wrote manuscript; E. S. O., H. H. N., I. K. managed project; S. P., X. G., Y. K., F. X. C., E. W., E. S. O., and H. H. N. conducted experiments. We thank Hyunseok Lee for drawing Figures 1(b), 2(c), and 3(a). We thank Soyeon Choi for the drawing in Figure 4(a).

Declaration of Conflicting Interests

The authors declared no potential conflicts of interest with respect to the research, authorship, and/or publication of this article.

Funding

The authors disclosed receipt of the following financial support for the research, authorship, and/or publication of this article: We thank funding sources from Advanced Bionics, Columbia University RISE (Research Initiative for Scientific Enhancement) Grant, and KAIST End Run Project Grant. This work was supported by Institute for Information & Communications Technology Promotion (IITP) grant funded by the Korea government (MSIT, Grant No. 2017-0-00052, Omni-sensory smart physical sensor original technology for human body sensing and diagnosis).This work was supported by Institute for Information & Communications Technology Promotion (IITP) grant funded by the Korea government (MSIT, Grant No. 2017-0-00052, Omni-sensory smart physical sensor original technology for human body sensing and diagnosis).

ORCID iD

Steve Park http://orcid.org/0000-0002-1428-592X

Supplemental Material

Supplementary material for this article is available online.

References

Åkerfeldt, M., Lund, A., & Walkenström, P. (2015). Textile sensing glove with piezoelectric PVDF fibers and printed electrodes of PEDOT: PSS. *Textile Research Journal*, *85*(17), 1789–1799. doi:10.1177/0040517515578333.

Cha, S., Kim, S. M., Kim, H., Ku, J., Sohn, J. I., Park, Y. J., . . . Kim, K. (2011). Porous PVDF as effective sonic wave driven nanogenerators. *Nano Letters*, *11*(12), 5142–5147. doi:10.1021/nl202208n.

Chocat, N., Lestoquoy, G., Wang, Z., Rodgers, D. M., Joannopoulos, J. D., & Fink, Y. (2012). Piezoelectric fibers for conformal acoustics. *Advanced Materials*, *24*(39), 5327–5332. doi:10.1002/adma.201201355.

Choi, S., & Jiang, Z. (2006). A novel wearable sensor device with conductive fabric and PVDF film for monitoring cardiorespiratory signals. *Sensors and Actuators A: Physical*, *128*(2), 317–326. doi:10.1016/j.sna.2006.02.012.

Crathorne, L., Bond, M., Cooper, C., Elston, J., Weiner, G., Taylor, R., & Stein, K. (2012). A systematic review of the effectiveness and cost-effectiveness of bilateral multichannel cochlear implants in adults with severe-to-profound hearing loss. *Clinical Otolaryngology*, *37*(5), 342–354. doi:10.1111/coa.12011.

Creighton, F. X., Guan, X., Park, S., Kymissis, I., Nakajima, H. H., & Olson, E. S. (2016). An intracochlear pressure sensor as a microphone for a fully implantable cochlear implant. *Otology & Neurotology*, *37*(10), 1596–1600. doi: 10.1097/MAO.0000000000001209.

Dickens, B., Balizer, E., Dereggi, A. S., & Roth, S. C. (1992). Hysteresis measurement of remanent polarization and coercive field in polymers. *Journal of Applied Physics*, *72*(9), 4258–4264. doi:10.1063/1.352213.

Inaoka, T., Shintaku, H., Nakagawa, T., Kawano, S., Ogita, H., Sakamoto, T., . . . Ito, J. (2011). Piezoelectric materials mimic the function of the cochlear sensory epithelium. *Proceedings of the National Academy of Sciences*, *108*(45), 18390–18395. doi:10.1073/pnas.1110036108.

Khan, S., Tinku, S., Lorenzelli, L., & Dahiya, R. S. (2015). Flexible tactile sensors using screen-printed P(VDF-TrFE) and MWCNT/PDMS composites. *IEEE Sensors Journal*, *15*(6), 3146–3155. doi:10.1109/jsen.2014.2368989.

Krajewski, A. S., Magniez, K., Helmer, R. J. N., & Schrank, V. (2013). Piezoelectric force response of novel 2D textile based PVDF sensors. *IEEE Sensors Journal*, *13*(12), 4743–4748. doi:10.1109/jsen.2013.2274151.

Lang, C., Fang, J., Shao, H., Ding, X., & Lin, T. (2016). High-sensitivity acoustic sensors from nanofibre webs. *Nature Communications*, *7*, 11108. doi:10.1038/ncomms11108.

Lee, H. S., Chung, J., Hwang, G. T., Jeong, C. K., Jung, Y., Kwak, J. H., . . . Lee, K. J. (2014). Flexible inorganic piezoelectric acoustic nanosensors for biomimetic artificial hair cells. *Advanced Functional Materials*, *24*(44), 6914–6921. doi:10.1002/adfm.201402270.

Lee, J. S., Shin, K. Y., Cheong, O. J., Kim, J. H., & Jang, J. (2015). Highly sensitive and multifunctional tactile sensor using free-standing ZnO/PVDF thin film with graphene electrodes for pressure and temperature monitoring. *Scientific Reports*, *5*, 7887. doi:10.1038/srep07887.

Li, G. R., Kagami, N., & Ohigashi, H. (1992). The possibility of formation of large ferroelectric domains in a copolymer of vinylidene fluoride and trifluoroethylene. *Journal of Applied Physics*, *72*(3), 1056–1061. doi:10.1063/1.351832.

Luo, C., Omelchenko, I., Manson, R., Robbins, C., Oesterle, E. C., Cao, G. Z., . . . Hume, C. R. (2015). Direct Intracochlear Acoustic Stimulation Using a PZT Microactuator. *Trends in Hearing*, *19*, 2331216515616942. doi:10.1177/2331216515616942.

Mao, Y., Zhao, P., McConohy, G., Yang, H., Tong, Y., & Wang, X. (2014). Sponge-like piezoelectric polymer films for scalable and integratable nanogenerators and self-powered electronic systems. *Advanced Energy Materials*, *4*(7), 1301624. doi:10.1002/aenm.201301624.

Nakajima, H. H., Dong, W., Olson, E. S., Merchant, S. N., Ravicz, M. E., & Rosowski, J. J. (2009). Differential intracochlear sound pressure measurements in normal human temporal bones. *Jaro-Journal of the Association for Research in Otolaryngology*, *10*(1), 23–36. doi:10.1007/s10162-008-0150-y.

Nilsson, E., Lund, A., Jonasson, C., Johansson, C., & Hagström, B. (2013). Poling and characterization of piezoelectric polymer fibers for use in textile sensors. *Sensors and Actuators A: Physical*, *201*, 477–486. doi:10.1016/j.sna.2013.08.011.

Olson, E. S. (1998). Observing middle and inner ear mechanics with novel intracochlear pressure sensors. *Journal of the Acoustical Society of America*, *103*(6), 3445–3463. doi: S0001-4966(98)00906-0.

Persano, L., Dagdeviren, C., Su, Y., Zhang, Y., Girardo, S., Pisignano, D., . . . Rogers, J. A. (2013). High performance piezoelectric devices based on aligned arrays of nanofibers of poly(vinylidenefluoride-co-trifluoroethylene). *Nature Communications*, *4*, 1633. doi:10.1038/ncomms2639.

Pfiffner, F., Prochazka, L., Péus, D., Dobrev, I., Dalbert, A., Sim, J. H., . . . Huber, A. (2017). A MEMS condenser microphone-based intracochlear acoustic receiver. *IEEE Transactions on Biomedical Engineering*, *64*(10), 2431–2438. doi:10.1109/TBME.2016.2640447.

Pi, Z., Zhang, J., Wen, C., Zhang, Z.-B., & Wu, D. (2014). Flexible piezoelectric nanogenerator made of poly(vinylidenefluoride-co-trifluoroethylene) (PVDF-TrFE) thin film. *Nano Energy*, *7*, 33–41. doi:10.1016/j.nanoen.2014.04.016.

Stöver, T., & Lenarz, T. (2009). Biomaterials in cochlear implants. *GMS Current Topics in Otorhinolaryngology, Head and Neck Surgery*, *8*, Doc 10. doi:10.3205/cto000062.

Wilson, B. S., & Dorman, M. F. (2008a). Cochlear implants: A remarkable past and a brilliant future. *Hearing Research*, *242*(1–2), 3–21. doi:10.1016/j.heares.2008.06.005.

Wilson, B. S., & Dorman, M. F. (2008b). Cochlear implants: Current designs and future possibilities. *Journal of Rehabilitation Research and Development*, *45*(5), 695–730. doi:10.1682/jrrd.2007.10.0173.

Xu, J., Dapino, M. J., Gallego-Perez, D., & Hansford, D. (2009). Microphone based on polyvinylidene fluoride (PVDF) micro-pillars and patterned electrodes. *Sensors and Actuators A: Physical*, *153*(1), 24–32. doi:10.1016/j.sna.2009.04.008.

Yip, M., Jin, R., Nakajima, H. H., Stankovic, K. M., & Chandrakasan, A. P. (2015). A fully-implantable cochlear implant SoC with piezoelectric middle-ear sensor and arbitrary waveform neural stimulation. *IEEE Journal of Solid-State Circuits*, *50*(1), 214–229. doi:10.1109/jssc.2014.2355822.

Yu, Y., Sun, H., Orbay, H., Chen, F., England, C. G., Cai, W., & Wang, X. (2016). Biocompatibility and in vivo operation of implantable mesoporous PVDF-based nanogenerators. *Nano Energy*, *27*, 275–281. doi:10.1016/j.nanoen.2016.07.015.

Zabek, D., Taylor, J., Boulbar, E. L., & Bowen, C. R. (2015). Micropatterning of flexible and free standing polyvinylidene difluoride (PVDF) films for enhanced pyroelectric energy transformation. *Advanced Energy Materials*, *5*(8), 1401891. doi:10.1002/aenm.201401891.

Zeng, F. G., Rebscher, S., Harrison, W., Sun, X., & Feng, H. (2008). Cochlear implants: System design, integration, and evaluation. *IEEE Reviews in Biomedical Engineering*, *1*, 115–142. doi:10.1109/RBME.2008.2008250.

Zhao, C., Knisely, K. E., & Grosh, K. (2017, 18–22 June). *Modeling, fabrication, and testing of a MEMS multichannel aln transducer for a completely implantable cochelar implant*. Paper presented at the 2017 19th International Conference on Solid-State Sensors, Actuators and Microsystems (TRANSDUCERS), Kaohsiung, Taiwan.

PVDF-based Piezoelectric Microphone for Sound Detection inside the Cochlea: Towards Totally Implantable Cochlear Implants

Steve Park,[1*] Xiying Guan,[2] Youngwan Kim,[3] Francis (Pete) X. Creighton,[2] Eric Wei,[4] Ioannis (John) Kymissis,[3*] Hideko Heidi Nakajima,[2*] Elizabeth S. Olson[4,5*]

Supplementary Information

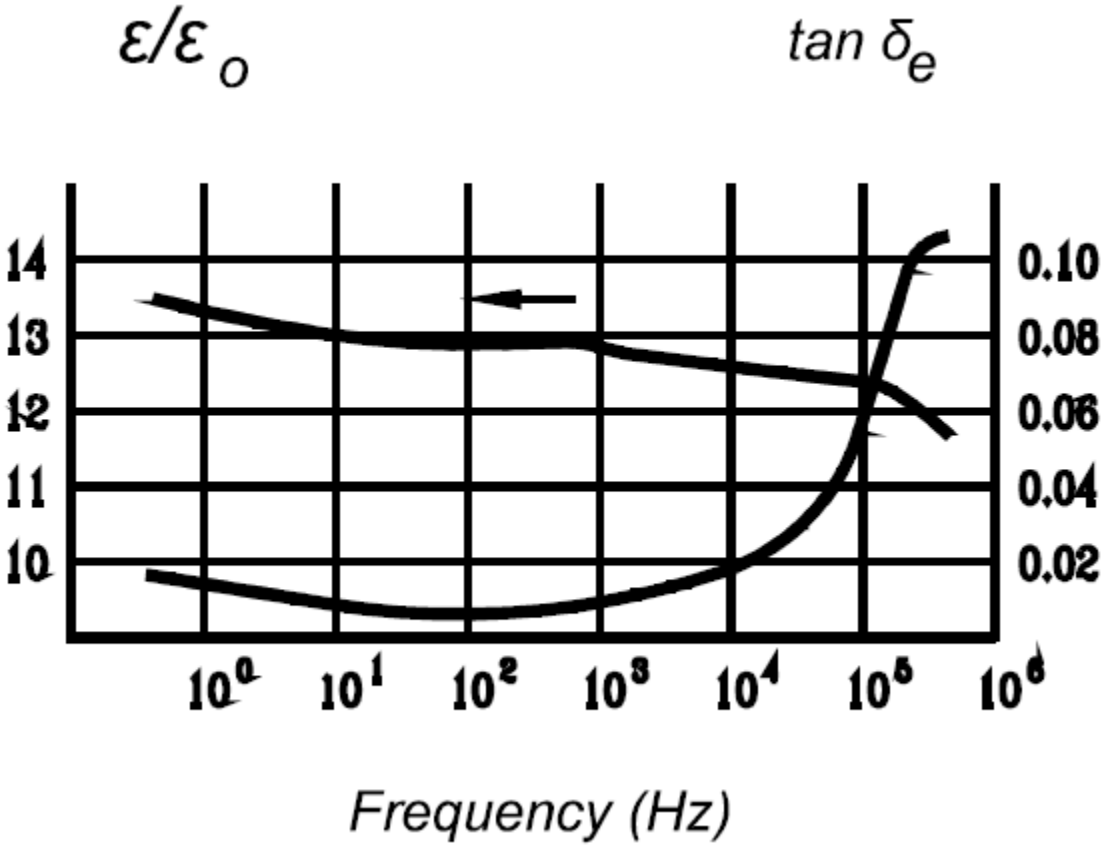

Fig. S1. Dielectric permittivity and dissipation factor versus frequency plot. Source: Measurement Specialties.

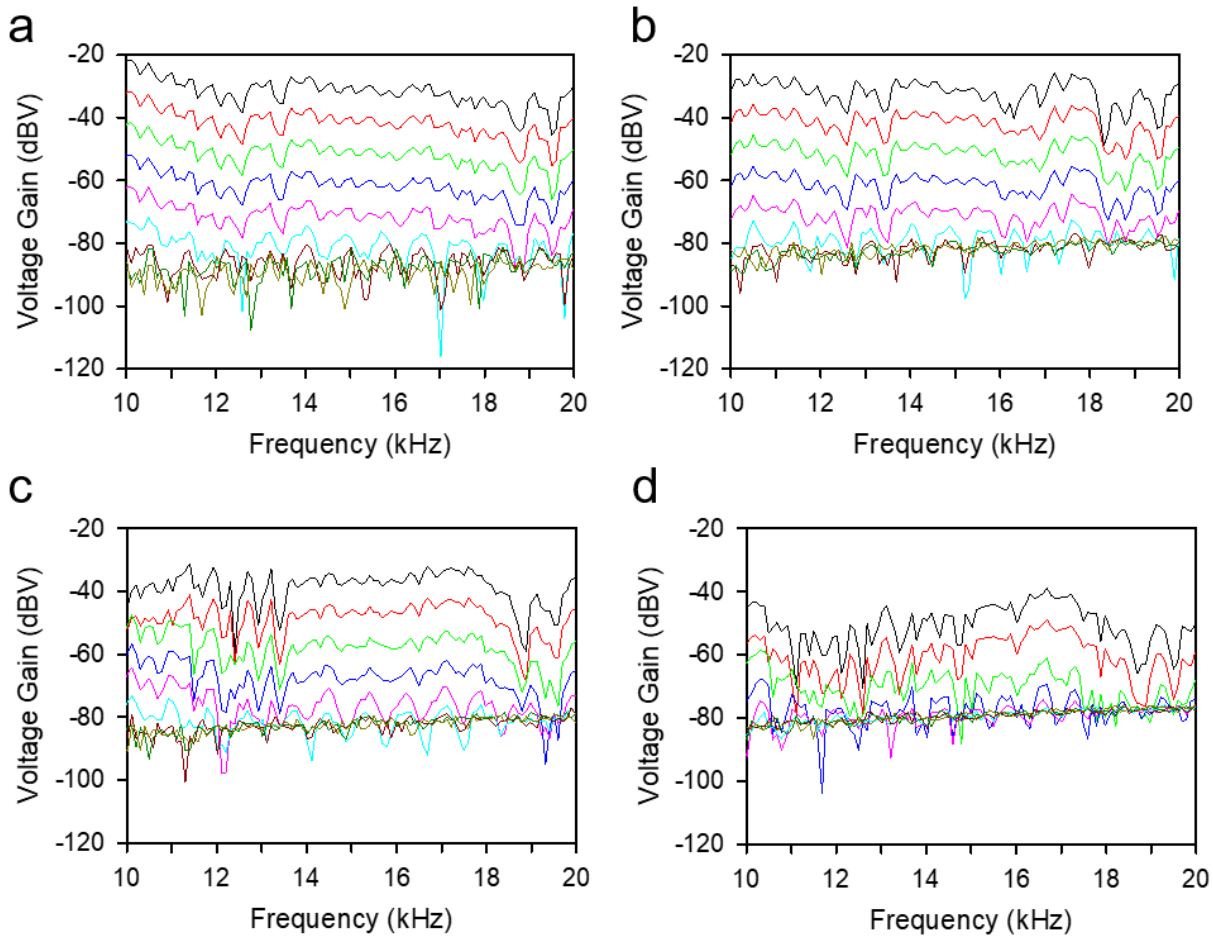

Fig. S2. Output voltage (after a gain of 1000) versus sound frequency for devices with active area equal to **a)** 40, **b)** 20, **c)** 10 , **d)** 1 mm^2. The experimental set-up is as described in Fig. 2c. The sound pressure level of 90 (black), 80 (red), 70(green), 60(blue), 50(pink), 40 (cyan), 30 (brown), 20 (dark green), noise (dark yellow) dB SPL was applied in succession. For devices with smaller active area, noise is reached at a higher sound pressure. These plots were used to graph Fig. 2d and 2e in the main text.

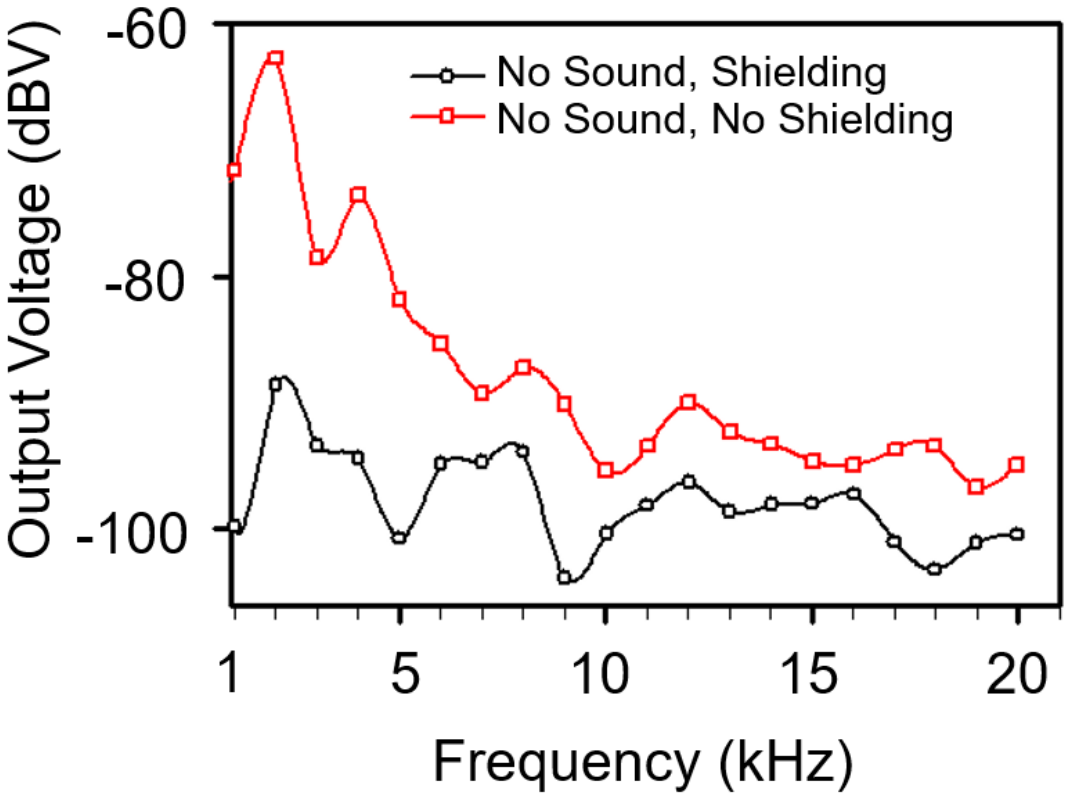

Fig. S3. PVDF device noise measurement (after a gain of 1000) with speaker on but with the sound blocked-off. The PVDF device was taped to a glass slide to restrict it to compression mode. The circle/black curve represents output voltage when the PVDF device was shielded from electromagnetic pick-up by placing it inside of a grounded aluminum box; whereas, the square/red curve represents output voltage of an unshielded PVDF device.